

Premixed Flame Propagation in High-Intensity Turbulence: Investigating the Role of Detailed Chemistry

Girish V. Nivarti and R. Stewart Cant
Department of Engineering, University of Cambridge
Cambridge, CB2 1PZ - United Kingdom

1 Background

The propagation of premixed flames in intense turbulence has been the subject of prolonged debate. The classical view is attributed to Damköhler [1] who proposed formulae for predicting turbulent flame speed (s_T) in two contrasting turbulent environments. When the unburned gas turbulence intensity (u') is weak compared with mixture laminar flame speed (s_L), the flame can be assumed to propagate normal to itself, locally, as a laminar flame. Hence, under these conditions the increase in turbulent flame speed is attributed solely to the change in area as follows

$$\frac{s_T}{s_L} = \frac{A_T}{A_L} \quad (1)$$

where A_T and A_L are the surface areas of turbulent and laminar flames respectively. In contrast, for the same turbulence integral length scale (ℓ_0), if the unburned gas turbulence intensity is much higher than the laminar flame speed ($u'/s_L \gg 1$), enhancement of diffusive effects within the flame alone governs the enhancement of turbulent flame speed. These two distinct regimes have been classified within a regime diagram [1] amongst several other regimes based on a few key dimensionless parameters. The lower turbulence case, pertinent to the following discussion, is known as the *flamelet* regime.

In recent years, much focus has been laid on identifying the changes that occur between these two fundamentally different regimes – in an intermediate regime known as the thin reaction zones (TRZ) regime. Turbulent flame stretch has been used to examine the burning state of a premixed turbulent flame within such regimes. Stretch can be quantified by a Karlovitz number (Ka) defined as

$$\text{Ka} = \left(\frac{u'}{s_L} \right)^{\frac{3}{2}} \left(\frac{\ell_0}{\delta_L} \right)^{-\frac{1}{2}} \quad (2)$$

where δ_L is the chemical length scale (the thermal flame thickness). Strict application of the Klimov-Williams criterion [1] indicates that the flamelet assumption is invalid when the Kolmogorov scale (η) is equal to the laminar flame thickness (δ_L), corresponding to $\text{Ka} = 1$. Nevertheless, flamelets have been observed in increasingly turbulent conditions [2]. Where flame propagation has not been predicted exactly by Eq. 1, corrections for the effects of turbulent strain have sufficed [3]. On the other hand, the

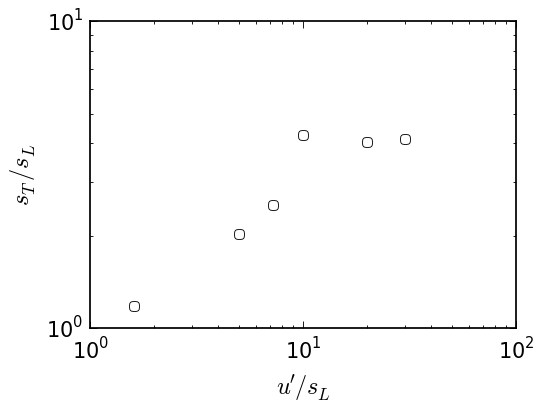


Figure 1: Turbulent flame speed variation ($s_T(u')$) obtained [8] using DNS with simplified chemistry.

existence of flamelet structure in the TRZ regime has been contested by recent measurements in Bunsen burners [4, 5] based on a study of propagation speed (s_T) and thermal flame thickness (δ_T).

Many different studies have, however, consistently established the *bending phenomenon* [6], which is the observation that the variation of turbulent flame speed with turbulence intensity ($s_T(u')$) becomes non-linear beyond a critical value of the turbulence intensity (u'_c). Since the critical turbulence intensity typically lies within the TRZ regime, a question arises: Can the bending phenomenon be explained by flamelet analysis? Recently, Direct Numerical Simulation (DNS) has been applied to challenging problems such as turbulence-chemistry interactions at the boundaries of TRZ regime [7].

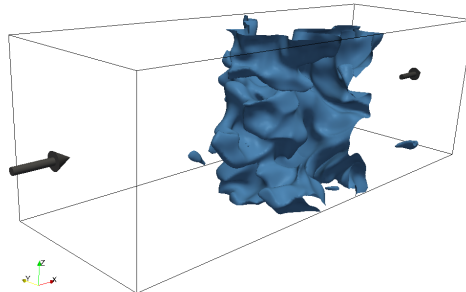


Figure 2: Flow configuration used in present DNS of turbulent premixed flames.

Previously, a parametric DNS study of stoichiometric methane-air flames was conducted [8] using single-step chemistry and the bending phenomenon was observed as shown in Fig. 1. The critical turbulence intensity was found to be ($u'_c \approx 10$) similar to recent experiments [9]. The objective of the work described in this paper is to investigate whether the bending phenomenon results solely from flame surface area destruction or from a change in internal flame structure. We conduct two separate simulations of turbulent premixed flames at the critical turbulence intensity (u'_c) a) with single-step chemistry and b) with detailed chemistry. The problem setup and results of these simulations have been compared in the following discussion.

2 Problem Setup and Numerical Approach

The problem domain, shown in Fig. 2, has dimensions $L_X/3 = L_Y = L_Z = 5$ mm with periodic boundaries in the span-wise directions. Inflow and outflow boundary conditions are specified in the streamwise direction, using the NSCBC formalism. A fully-compressible 3D formulation of the Navier-Stokes equations is solved using the DNS code SENG2. A 10^{th} -order centred finite difference operator is used to evaluate the spatial derivatives at each mesh point. Time-advancement is effected using a low-storage 4^{th} -order explicit Runge-Kutta method. Further details and references for the numerical approach are provided in a recent paper [8].

Case	Mechanism	Steps	Transport	Species	δ_L (mm)	s_L (cm s ⁻¹)	τ_c (ms)
I	Single-step [10]	1	Le = 1	1	0.36	37.08	0.93
II	Detailed [11]	35[10R]	Mixture Averaged	16	0.41	42.72	0.97

Table 1: Laminar 1D premixed methane-air flame properties.

A planar laminar flame solution calculated *a priori* is prescribed at $x = L_X/2$ specifying the initial thermo-chemical state throughout the domain. The inlet temperature, pressure and mean velocity are $p_0 = 1$ bar, $T_0 = 300$ K, and $\langle u_0 \rangle = 0.39$ ms⁻¹ respectively. Key properties of laminar flame solutions obtained under these conditions using single-step and detailed chemical mechanisms have been tabulated in Table 1. The single-step mechanism [10] is based on Arrhenius parameters reported earlier [8], whereas a 35-step (including 10 reversible reactions), 16 species chemical mechanism [11] provides the detailed chemistry. As the flame develops during the course of the simulation, the chosen stream-wise extent serves to minimize interactions between the flame and inflow-outflow boundaries.

Case	u'_0 (ms ⁻¹)	ℓ_0 (mm)	η (μ m)	Δx (μ m)	τ_0 (ms)	Re _T	Ka	Da	s_T/s_L
I							16.5	0.4	4.0
II	3.9	1.3	33.1	52.3	0.3	332.4	14.7	0.5	2.5

Table 2: Simulation inlet parameters and computed reactive flow properties.

The initial turbulent flow-field is first constructed from the Batchelor-Townsend energy spectrum function using a spectral method [8]. Time-varying inflow boundary conditions required to sustain the turbulence are imposed using an *a priori* calculated solution of homogeneous isotropic decaying turbulence using the same energy spectrum as for initialisation. A frozen state of the precursor simulation is then scanned to produce a time varying turbulent flow-field at the inlet plane using Taylor's hypothesis.

The DARWIN computing cluster at the University of Cambridge with two 2.60 GHz eight core Intel Sandy Bridge E5-2670 processors per node has been used for all computations. The problem domain was decomposed into $12 \times 4 \times 4 = 192$ sub-domains, each allotted to a separate core on the cluster. The single-step case required 32 hours of computation, while the complex chemistry simulation needed nearly 360 hours with the same parallel decomposition to solve up to $t \approx 3\tau_0$ eddy turn-over times.

3 Results

In the following analysis, a progress variable based defined as $c = (Y_u^f - Y^f)/(Y_u^f - Y_b^f)$ where Y_u^f and Y_b^f represent the unburnt and burnt fuel mass fractions respectively. In Fig. 3, normalized turbulent flame speed (s_T/s_L) is plotted against normalized flame surface area (A_T/A_L) for three different c isosurfaces (0.1, 0.5, 0.9). The observed variation deviates from Eq. 1 (blue line) but retains linearity until a certain isosurface area is attained. Low flame speeds and flame surface areas are observed in case

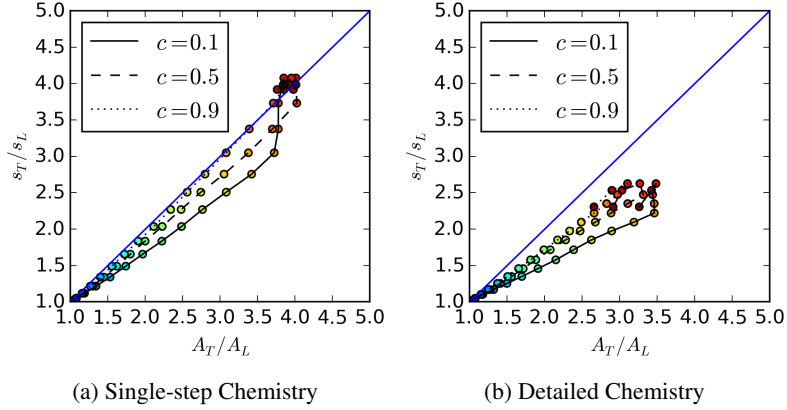


Figure 3: Turbulent flame speed variation with flame surface area. Coloured dots indicate time (blue for $t = 0$ to red for $t = 3\tau_0$). Eq. 1 is shown as a blue line.

II (detailed chemistry) with the net effect being a larger deviation from Eq. 1. Within the time frame $2\tau_0 < t < 3\tau_0$, an area destruction event occurs which causes all c isosurfaces to collapse together. This is a consequence of the small size of the DNS domain, which is able to encompass only a small number of large-scale flame structures (see Fig. 2). The flame is observed to recover and to begin another period of linear growth; this will be investigated in subsequent work.

The flame surface density function (SDF) at $t = 3\tau_0$ has been plotted in Fig. 4. The scatter displays a significant variation at any c isosurface, but compared with the single-step chemistry results, the detailed chemical mechanism shows a greater degree of scatter at each c isosurface. Moreover, the detailed chemistry SDF is skewed towards the products, similar to previous DNS work [12], whereas the simplified chemistry results appear to be symmetric about $c = 0.5$, comparable to recent experiments [13]. These SDF variations may be understood as manifestations of curvature and strain effects [2].

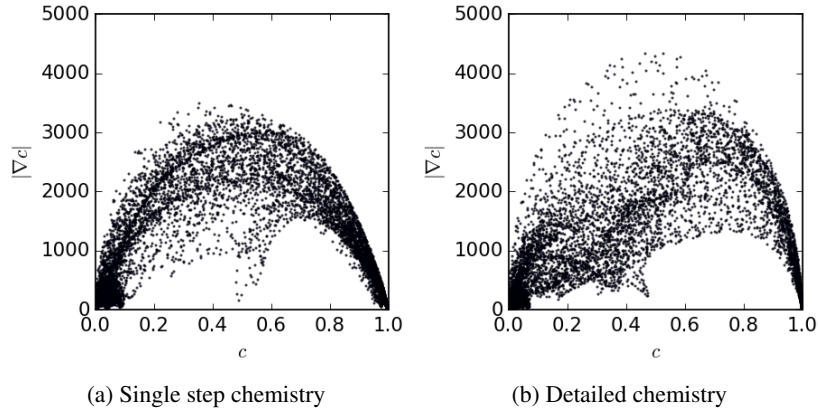


Figure 4: Variation of surface density function across the flame.

We define the curvature and tangential strain rate as follows

$$\text{Curvature, } \kappa = \nabla \cdot \hat{n} \quad (3)$$

$$\text{Tangential Strain, } a_T = \nabla \cdot \mathbf{v} - \hat{n}\hat{n} : \nabla \mathbf{v} \quad (4)$$

where \mathbf{v} is the velocity vector and \hat{n} is the flame surface normal vector.

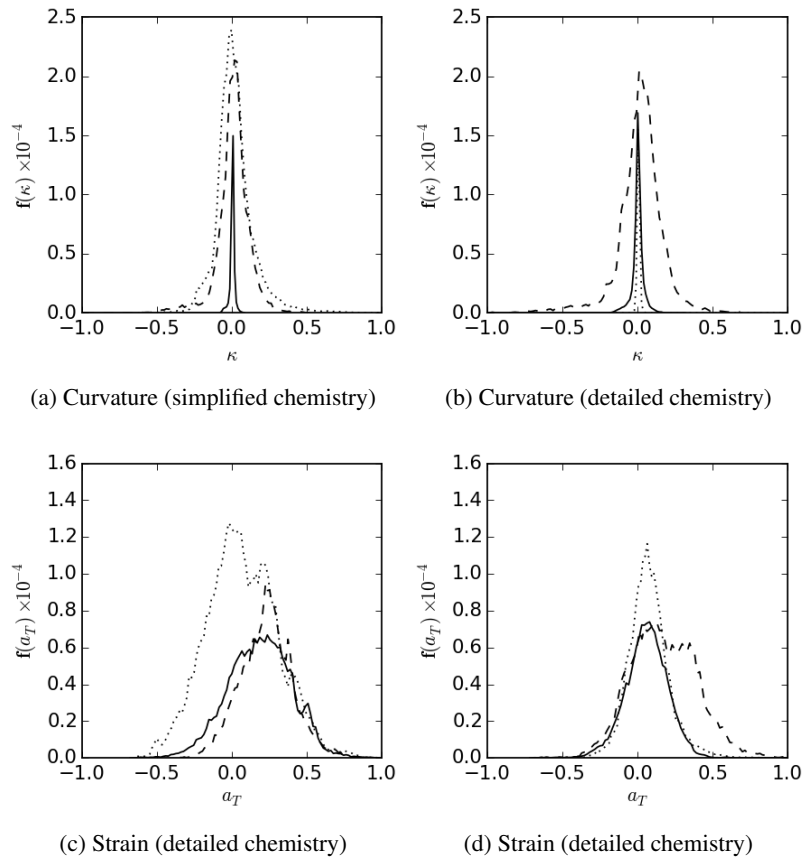


Figure 5: Curvature (κ) probability density function for both single-step and detailed chemistry. Solid line is $c = 0.1$, dashes represent $c = 0.5$, and $c = 0.9$ is marked by dots.

Fig. 5 illustrates the similarity between PDFs of curvature (κ) obtained for both single-step and detailed chemistry simulations. Each PDF bears a resemblance also to those observed in early DNS calculations of weakly turbulent premixed flames in the flamelet regime [3]. At each c isosurface, the mean curvature is $\langle \kappa \rangle_{c=c^*} = 0$, the curves are symmetric and have a sharp distinctive peak at zero with little deviation from the mean. This is contrary to the deviations observed in high-intensity turbulence [13], suggesting that deviations may not rise monotonically with turbulence intensity. Fig. 5 shows the PDF of tangential strain rate for case I (single-step) and II (detailed chemistry). It is noted that the probability of positive tangential strain rate is high in both cases as with previous DNS work [12], and that the overall distribution is similar. These distributions indicate the similarities in the underlying physical processes that influence turbulent flame speed for both single-step and detailed chemistry simulations.

Mass fractions of OH and CH₂O radicals have been identified on a stream-wise plane ($x - y$) and are shown in Fig. 6. The snapshots show considerable flame break-up; however, the internal chemical structure appears intact. Flame surface-density markers will be analysed in subsequent work.

4 Conclusions

Direct Numerical Simulations of a freely-propagating turbulent premixed flame were conducted using single-step and detailed chemistry while maintaining the turbulence intensity ($u'/s_L \approx 10$) approximately at the turbulence intensity (u'_c) corresponding to the onset of bending. It appears from various

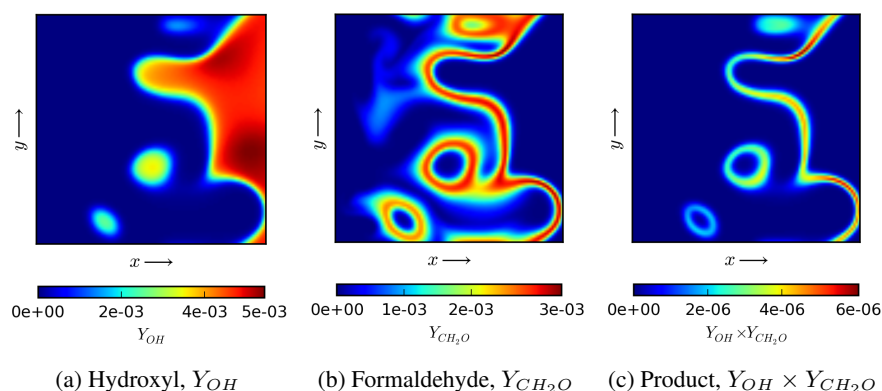


Figure 6: Radical species (OH and CH_2O) identified on a stream-wise plane indicating flame position.

comparisons that both simplified and realistic flames exhibit similar properties in the vicinity of bending. Comparison of flame surface curvature and strain support the deduction that, even at $u'/s_L \approx 10$, turbulent flame speed may be solely a function of flame surface area. Further investigations will help confirm these preliminary observations.

References

- [1] Peters, N. (2000). *Turbulent combustion*. Cambridge University Press.
- [2] Driscoll, J. F. (2008). Turbulent premixed combustion: Flamelet structure and its effect on turbulent burning velocities. *Progress in Energy and Combustion Science*, 34, pp. 91–134.
- [3] Bray, K. N. C., and Cant, R. S. (1991). Some applications of Kolmogorov's turbulence research in the field of combustion. *Proceedings of the Royal Society A: Mathematical, Physical and Engineering Sciences*, 434, pp. 217–240.
- [4] Chen, Y., and Bilger, R. W. (2001). Simultaneous 2-D imaging measurements of reaction progress variable and OH radical concentration in turbulent premixed flames: Experimental methods and flame brush structure. *Combustion Science and Technology*, 167, pp. 131–167.
- [5] Yuen, F. T., and Gülder, O. L. (2013). Turbulent premixed flame front dynamics and implications for limits of flamelet hypothesis. *Proceedings of the Combustion Institute*, 34, pp. 1393–1400.
- [6] Lipatnikov, A., and Chomiak, J. (2002). Turbulent flame speed and thickness: phenomenology, evaluation, and application in multi-dimensional simulations. *Progress in Energy and Combustion Science*, 28, pp. 1–74.
- [7] Poludnenko, A. Y., and Oran, E. (2011). The interaction of high-speed turbulence with flames: Turbulent flame speed. *Combustion and Flame*, 158, pp. 301–326.
- [8] Nivarti, G. V., and Cant, R. S. (2015). Aerodynamic quenching and burning velocity of turbulent premixed methane-air flames. In Proceedings of ASME Turbo Expo 2015: Turbine Technical Conference and Exhibition. (Submitted).
- [9] Shy, S. S., Lin, W., and Peng, K. (2000). High-intensity turbulent premixed combustion: General correlations of turbulent burning velocities in a new cruciform burner. *Proceedings of the Combustion Institute*, 28, pp. 561–568.
- [10] Poinso, T., and Veynante, D. (2006). *Theoretical and numerical combustion*. Edwards.
- [11] Giovangigli, V., and Smooke, M. D. (1987). Extinction of strained premixed laminar flames with complex chemistry. *Combustion Science and Technology*, 53, pp. 23–49.
- [12] Chakraborty, N., and Cant, R. S. (2004). Unsteady effects of strain rate and curvature on turbulent premixed flames in an inflow-outflow configuration. *Combustion and Flame*, 137, pp. 129–147.
- [13] Gülder, O., and Smallwood, G. (2007). Flame surface densities in premixed combustion at medium to high turbulence intensities. *Combustion Science and Technology*, 179, pp. 191–206.